Towards quantitative digital subtraction perfusion angiography

An animal study

Su, Ruisheng; van der Sluijs, P. Matthijs; Bobi, Joaquim; Taha, Aladdin; van Beusekom, Heleen M.M.; van der Lugt, Aad; Niessen, Wiro J.; Ruijters, Danny; van Walsum, Theo

DOI
10.1002/mp.16473

Publication date
2023

Document Version
Final published version

Published in
Medical Physics

Citation (APA)
Su, R., van der Sluijs, P. M., Bobi, J., Taha, A., van Beusekom, H. M. M., van der Lugt, A., Niessen, W. J., Ruijters, D., & van Walsum, T. (2023). Towards quantitative digital subtraction perfusion angiography: An animal study. *Medical Physics*, *50*(7), 4055-4066. https://doi.org/10.1002/mp.16473

SGRT

USE OF **SURFACE GUIDANCE** TO HELP IMPROVE THE SAFETY, EFFECTIVENESS AND EFFICIENCY OF THE *ENTIRE* **RADIATION THERAPY** WORKFLOW

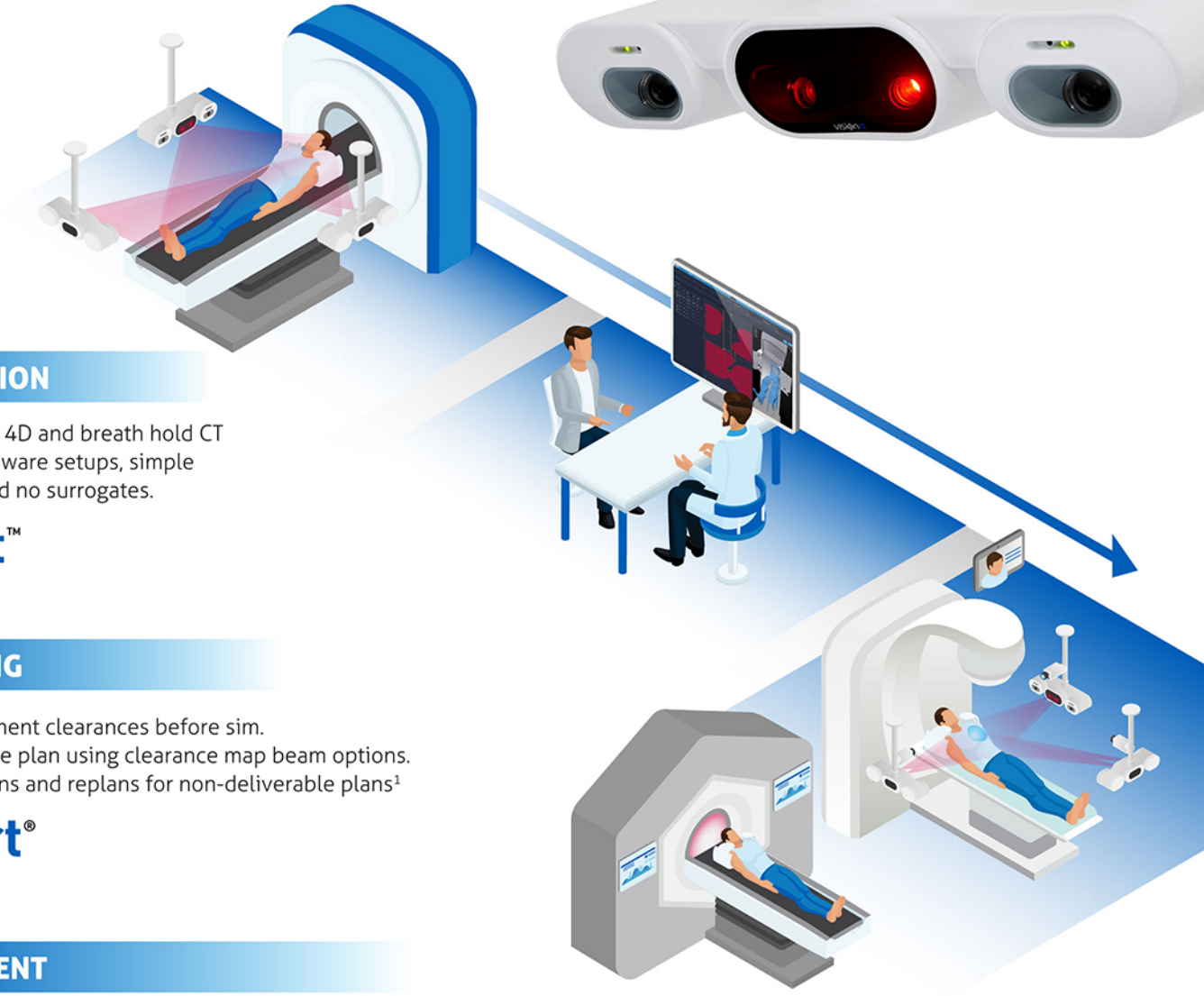

SIMULATION

Non-contact 4D and breath hold CT with no hardware setups, simple workflow and no surrogates.

simrt™

PLANNING

Check treatment clearances before sim.
Improve dose plan using clearance map beam options.
Avoid dry runs and replans for non-deliverable plans[1]

maprt®

TREATMENT

Contactless patient ID prior to treatment.
Demonstrated rapid patient setup without the need for tattoos.
TG302/ESTRO-ACROP compliant motion monitoring accuracy at all couch / gantry angle and skin tones.

alignrt® **alignrt® *InBore™***

Dose visualization can help stop treatment errors in real-time.*

dosert™
Powered by BeamSite®

1.Sheng Ke. Surface guided clearance mapping: see more, do more and achieve more. SGRT Community USA 2022

visionrt

0008-0038 - SGRT Workflow Ad v1.0

Received: 22 September 2022 | Revised: 9 April 2023 | Accepted: 20 April 2023

DOI: 10.1002/mp.16473

RESEARCH ARTICLE

MEDICAL PHYSICS

Towards quantitative digital subtraction perfusion angiography: An animal study

Ruisheng Su[1] | **P. Matthijs van der Sluijs**[1] | **Joaquim Bobi**[2] | **Aladdin Taha**[2] | **Heleen M.M. van Beusekom**[2] | **Aad van der Lugt**[1] | **Wiro J. Niessen**[1,3] | **Danny Ruijters**[4] | **Theo van Walsum**[1]

[1]Department of Radiology & Nuclear Medicine, Erasmus MC, University Medical Center, Rotterdam, The Netherlands

[2]Department of Experimental Cardiology, Erasmus MC, University Medical Center, Rotterdam, The Netherlands

[3]Faculty of Applied Sciences, Delft University of Technology, Delft, The Netherlands

[4]Philips Healthcare, Best, The Netherlands

Correspondence
Ruisheng Su, Department of Radiology and Nuclear Medicine, Erasmus MC, University Medical Center, Rotterdam, The Netherlands.
Email: r.su@erasmusmc.nl

Code has been made available at https://gitlab.com/radiology/igit/q-maestro/perfusionDSA.

Funding information
Health Holland, Grant/Award Numbers: LSHM17016, EMCLSH19006; Hartstichting, Grant/Award Number: CVON2015-01; Brain Foundation Netherlands, Grant/Award Number: HA2015.01.06

Abstract

Background: X-ray digital subtraction angiography (DSA) is the imaging modality for peri-procedural guidance and treatment evaluation in (neuro-) vascular interventions. Perfusion image construction from DSA, as a means of quantitatively depicting cerebral hemodynamics, has been shown feasible. However, the quantitative property of perfusion DSA has not been well studied.

Purpose: To comparatively study the independence of deconvolution-based perfusion DSA with respect to varying injection protocols, as well as its sensitivity to alterations in brain conditions.

Methods: We developed a deconvolution-based algorithm to compute perfusion parametric images from DSA, including cerebral blood volume (CBV_{DSA}), cerebral blood flow (CBF_{DSA}), time to maximum (Tmax), and mean transit time (MTT_{DSA}) and applied it to DSA sequences obtained from two swine models. We also extracted the time intensity curve (TIC)-derived parameters, that is, area under the curve (AUC), peak concentration of the curve, and the time to peak (TTP) from these sequences. Deconvolution-based parameters were quantitatively compared to TIC-derived parameters in terms of consistency upon variations in injection profile and time resolution of DSA, as well as sensitivity to alterations of cerebral condition.

Results: Comparing to TIC-derived parameters, the standard deviation (SD) of deconvolution-based parameters (normalized with respect to the mean) are two to five times smaller, indicating that they are more consistent across different injection protocols and time resolutions. Upon ischemic stroke induced in a swine model, the sensitivities of deconvolution-based parameters are equal to, if not higher than, those of TIC-derived parameters.

Conclusions: In comparison to TIC-derived parameters, deconvolution-based perfusion imaging in DSA shows significantly higher quantitative reliability against variations in injection protocols across different time resolutions, and is sensitive to alterations in cerebral hemodynamics. The quantitative nature of perfusion angiography may allow for objective treatment assessment in neurovascular interventions.

KEYWORDS
cerebral blood volume, deconvolution, digital subtraction angiography, ischemic stroke, perfusion imaging, swine, time intensity curve

1 | INTRODUCTION

Visualization and quantification of cerebral hemodynamics is essential in the diagnosis of neurovascular diseases, such as vessel occlusion, vessel stenosis, and vasospasm, and the evaluation of endovascular treatment. Such quantifications include the construction of parametric maps of cerebral blood volume (CBV), cerebral blood flow (CBF), time to maximum (Tmax), and mean transit time (MTT), which are generally obtained via perfusion imaging, a functional imaging technique mainly used in the diagnosis of acute ischemic stroke and oncology. With perfusion imaging the temporal information on contrast material in vessels and brain tissue is depicted, highlighting the underlying functional characteristics of the brain. Perfusion imaging has been performed with well-established image modalities such as computed tomography (CT)[1–4] and Magnetic Resonance Imaging (MRI).[5–7]

X-ray digital subtraction angiography (DSA) is the imaging modality used for fast and accurate periprocedural guidance in (neuro-) vascular interventions, including blood flow visualization. During endovascular treatment of large vessel occlusions in patients with acute ischemic stroke, DSA primarily guides the navigation of catheters and aids in the assessment of treatment effects after an attempt of thrombus retrieval. The preference for DSA, especially in endovascular treatments, is attributed to its minimally invasive and real-time nature, low cost, fast acquisition, relatively low risk, and the ability to stand next to the patient while acquiring imaging. Additionally, in contrast to MRI and CT, DSA provides excellent spatio-temporal resolution, thus offering high-quality visualization of flow characteristics as well as vascular abnormalities.

Despite the popularity of DSA in current clinical practice, its usage largely remains qualitative. For example, in the evaluation of endovascular thrombectomy (EVT) for acute ischemic stroke, interventionalists visually inspect the DSA series frame by frame, back and forth, and extract a subjective and coarse Thrombolysis in Cerebral Infarction (TICI) score[8–11] to report the degree of brain tissue reperfusion. A few works have recently investigated quantitative evaluation of DSA series in EVT. Su *et al.* proposed an automatic framework for quantitative TICI scoring.[12] Deep learning approaches have recently been applied on DSA for intracranial aneurysm detection,[13] phase classification,[12] TICI classification,[14] vessel perforation detection,[15] image generation,[16–19] thrombus classification,[20] vessel segmentation,[21–23] and artery/vein separation.[24] Nevertheless, most existing studies do not quantitatively assess cerebral hemodynamics.

While perfusion imaging techniques are extensively adopted for MRI and CT, with even FDA-approved software deployed in clinical routines, its applicability and potential value in DSA may have been underestimated by the clinical community. This may be partially caused by the projective nature of 2D DSA series, posing extra challenges in mapping flow-based parameters to realistic blood volume and flow information. To distinguish these DSA parameters from the 3D variants, we therefore deliberately use the DSA subscript in CBV_{DSA}, CBF_{DSA}, and MTT_{DSA}.

The concept of perfusion DSA was first proposed in 2005 by Bogunovic *et al.* [25] using the maximum slope model.[26] Subsequently in 2010, Strother *et al.* [27] demonstrated that the color-coded parametric images in DSA enhances the ease in visual treatment evaluation. Such angiographic parameters were extracted directly from time intensity curves (TICs) which are dependent on the contrast injection profile. In 2015, Scalzo et al. [28] applied the well-established singular value decomposition (SVD) deconvolution-based algorithms and demonstrated the feasibility of constructing color-coded normalized parametric images of CBV_{DSA}, CBF_{DSA}, and MTT_{DSA} from DSA images. In recent years, the utility of various angiographic parametric images has been showcased in a number of applications, for example in assessing vasospasm,[29] chronic mesenteric ischemia,[30] and cerebral ischemic core.[31]

Although it has been shown that perfusion DSA is feasible, few studies have investigated the impact of injection protocols on angiographic perfusion parameters in in-vivo DSA. A recent phantom study by Rava et al. [32] demonstrated the independence of SVD-based parameters with respect to different injection rates. The phantom experiments assumed ideal scenarios and focused on assessing a few proximal arteries without considering venous vessels or parenchymal perfusion. A few studies have nevertheless evidenced the fact that TIC-derived parameters are strongly dependent on injection parameters. Ahmed et al. investigated the impact of injection parameters on TIC-derived parameters and reported a proportional correlation between injection volume and TIC characteristics (i.e., peak, AUC, and TTP).[33] Takagi et al. studied the relationship between injection rate and contrast enhancement on 3D DSA images.[34] Quantitative assessment of deconvolution-based and TIC-derived parameters may promote further applications of perfusion DSA in clinical practice. This work extends existing phantom studies to an in-vivo situation and further investigates the quantitative property of deconvolution-based perfusion DSA in arteries, veins, and parenchymal regions on realistic DSA acquisitions. Specifically, we use swine models to study the independence of deconvolution-based perfusion parameters against TIC-derived parameters across different injection profiles. Furthermore, we induced ischemic stroke in a swine model to validate the sensitivity of perfusion DSA to alterations in brain hemodynamic conditions.

2 | METHODS

2.1 | X-ray DSA imaging model

Cerebral X-ray angiography produces a 2D image showing the attenuation of X-rays through the brain. Assuming the incident photon intensity I_0, the observed intensity $I(x, y)$ depends on the thickness $d_b(x, y)$ and attenuation coefficient of brain structures $\mu_b(x, y)$, as described based on Lambert-Beer's law in

$$I(x, y) = I_0 e^{-(\mu_b d_b(x,y)}. \quad (1)$$

In order to enhance cerebral vessels from the surrounding tissue, contrast agent is injected, which leads to various levels of increased attenuation along photon trajectories. The pixel intensity at (x,y) then becomes

$$I(x, y) = I_0 e^{-[\mu_b d_b(x,y)+\mu_c d_c(x,y)]}, \quad (2)$$

where μ_c and $d_c(x, y)$ denote the attenuation coefficient of contrast material and its thickness (i.e., vessel thickness) respectively. To eliminate the disturbance of background structures (e.g., skull, teeth) and visualize only the vessels and perfused tissue, each contrasted frame is first logarithmically transformed and then subtracted by the non-contrasted logarithmically transformed mask frame, which gives

$$\begin{aligned} I_{DSA}(x, y) &= \ln\left(I_{contrasted}(x, y)\right) - \ln\left(I_{mask}(x, y)\right) \\ &= -[\mu_b d_b(x, y) + \mu_c d_c(x, y)] - [-(\mu_b d_b(x, y)] \\ &= -\mu_c d_c(x, y). \end{aligned}$$

In this way, the DSA image is independent of the brain anatomy and its intensity linearly correlates with the summed contrast agent concentration of brain tissue along the photon trajectory. For a 2D+t DSA series, cerebral flow and perfusion can thus be derived.

2.2 | Perfusion angiography

From the time axis of a DSA series, a TIC can be extracted from each pixel. As illustrated in Figure 1, a few perfusion parameters describe the characteristics of a TIC. Each parameter compresses the time dimension of DSA series into a single value, such that the 2D+t DSA series collapses to a 2D parametric image. Note that a TIC in DSA is likely a mixture of TICs along the photon trajectory. The resulting projective parametric images reflect integrated perfusion properties of overlapping brain voxels.

TABLE 1 Definitions of perfusion parameters

Parameter	Definition
AUC	Area under the contrast concentration curve
TTP	Time to the maximum of the contrast concentration curve
Peak	The maximum of contrast concentration
CBV_{DSA}	Cerebral blood volume represented as the area under the residue function
CBF_{DSA}	Cerebral blood flow represented as the maximum of the residue function
Tmax	Time to the maximum of the flow-scaled residue function
MTT_{DSA}	Mean transit time represented by CBV_{DSA} divided by CBF_{DSA}, referring to the average time period that contrast spends in the area of interest.

2.2.1 | TIC-derived parameters

Parameters that directly describe the TIC include area under the curve (AUC), peak concentration, and time-to-peak (TTP) (Table 1). These parameters can be easily computed. However, their quantitative consistency typically suffers from variations in injection protocol, for example, injection volume, flow, duration, and contrast material concentration. Contrast injection is often manual in clinical practice, thus inevitably variable. This may pose additional challenges when comparing these TIC-derived parameters from the same patient acquired at different time points or patient conditions.

2.2.2 | Deconvolution-based parameters

CBV, CBF, Tmax, and MTT (Table 1) are widely adopted perfusion parameters that are related to the intrinsic microcirculation properties in tissues and (micro-) vessels. Methods to compute these parameters in cerebral imaging modalities (e.g., MRI, CT) are generally deconvolution-based or sometimes direct measurement-based. Similar deconvolution-based approaches can also be employed on DSA series to derive parametric images.[28]

The deconvolution-based method is grounded on the indicator-dilution theory,[35] which in principle states that the contrast concentration at the volume of interest $C_{\text{voi}}(t)$ is proportional to the volume flow CBF and the residual concentration within the volume of interest, represented by the contrast concentration of the input artery (C_{art}) convolved with a residue function $r(t)$:

$$C_{\text{voi}}(t) = \text{CBF} \cdot \rho_{\text{voi}} \cdot (C_{\text{art}} * r)(t). \quad (3)$$

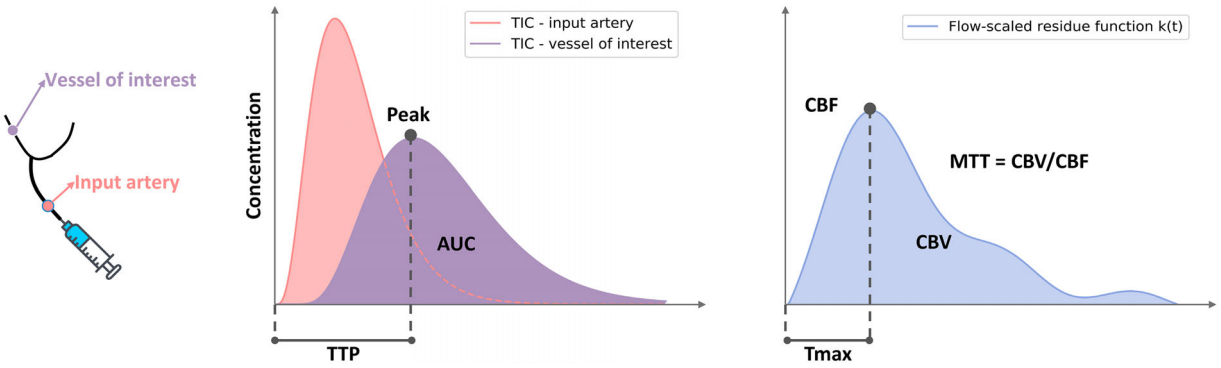

FIGURE 1 Overview of TIC-derived and deconvolution-based perfusion parameters. k(t) denotes the flow-scaled residue function as referred to in Equation (4) of Section 2.2.2 It can be obtained from the TIC of the vessel deconvolved with the TIC of the input artery. TIC-derived parameters are TTP, peak concentration, and area under the curve (AUC). Deconvolution-based parameters include CBV_{DSA}, CBF_{DSA}, T_{max}, and MTT_{DSA}. CBF, cerebral blood flow; CBV, cerebral blood volume; MTT, mean transit time; DSA, digital subtraction angiography; TIC, time intensity curve; TTP, time-to-peak.

ρ_{voi} denotes the mean intensity of the volume of interest. Detailed derivations of this formulation can be found elsewhere.[36,37]

To compute the value of CBF, Equation (3) can be rearranged to

$$C_{\text{voi}}(t) = (C_{\text{art}} * (\text{CBF} \cdot \rho_{\text{voi}} \cdot r))(t). \tag{4}$$

As $C_{\text{voi}}(t)$ and $C_{\text{art}}(t)$ are known from TICs (see Figure 1), $(\text{CBF} \cdot \rho_{\text{voi}} \cdot r)(t)$, known as the flow-scaled residue function $k(t)$, can be directly resolved from a deconvolution. With the assumption that CBF is constant, CBF can be determined as

$$\text{CBF} = \frac{1}{\rho_{\text{voi}}} \cdot \max(k(t)), \tag{5}$$

by taking peak time point of $k(t)$ and $r(t)$, where $\max(r(t)) = 1$.[37] This time point is known as Tmax. Subsequently, CBV can be further deduced from the flow-scaled residue function $k(t)$ as

$$\text{CBV} = \frac{1}{\rho_{\text{voi}}} \cdot \int_0^{\text{inf}} k(\tau) d\tau. \tag{6}$$

Finally, we compute the MTT based on the central volume theorem[2,38] as follows

$$\text{MTT} = \frac{\text{CBV}}{\text{CBF}}. \tag{7}$$

2.3 | The swine model

Deconvolution-based computation of perfusion parameters relies on the arterial input function (AIF), which is the TIC of a contrast input artery. Figure 2 shows the swine brain vasculature: the contrast agent flows from a proximal artery, passes through a mesh-like structure, named rete mirabile, enters the internal carotid artery (ICA) and middle cerebral artery (MCA), irrigates the brain tissues and eventually leaves the brain via veins. The rete mirabile is a mesh of small vessels present in several large mammals but not in humans. To circumvent the unknown effect of rete mirabile on perfusion DSA, the AIF was extracted from the ICA branch following the rete mirabile to best simulate the human brain (Figure 2a). To reduce the noise of TICs per pixel, we applied temporal Gaussian filtering preceding the SVD-based deconvolution. When evaluating tissue level parameters, Frangi filter[39] and proper thresholds were applied to exclude vessels in the parenchymal area (Figure 2a).

With the goal of evaluating the independence and sensitivity of deconvolution-based parameters, we perform an animal study using two swine models. This study has been approved by the animal ethics committee of the Erasmus MC, University Medical Center, Rotterdam, The Netherlands (AVD1010020198546), and complied with the EU Directive 2010/63/EU for animal experimentation with scientific purposes. Two female Yorkshire-Landrace swine underwent selective brain angiography to study DSA-derived CBF patterns in healthy (n = 1, 60.7 kg) and altered conditions (MCA occlusion) (n = 1, 49.7 kg). Both animals were sedated with Zoletil (6 mg/kg), Xylazine (2.25 mg/kg) and Atropine (30 g/kg), anesthetized with Propofol (2–10 mg/kg/h) and Sufentanyl (0.5–3 mcg/kg/h) and mechanically ventilated during the whole procedure. Heart rate, invasive arterial pressure, peripheral saturation and end-tidal CO_2 were continuously monitored during the experiment. Endovascular cannulation of the ICA was not feasible in swine due to the physiological presence of a complex network of anastomosing small vessels (rete mirabile)[40] between the common carotid artery and the ICA. To obtain selective brain angiography,

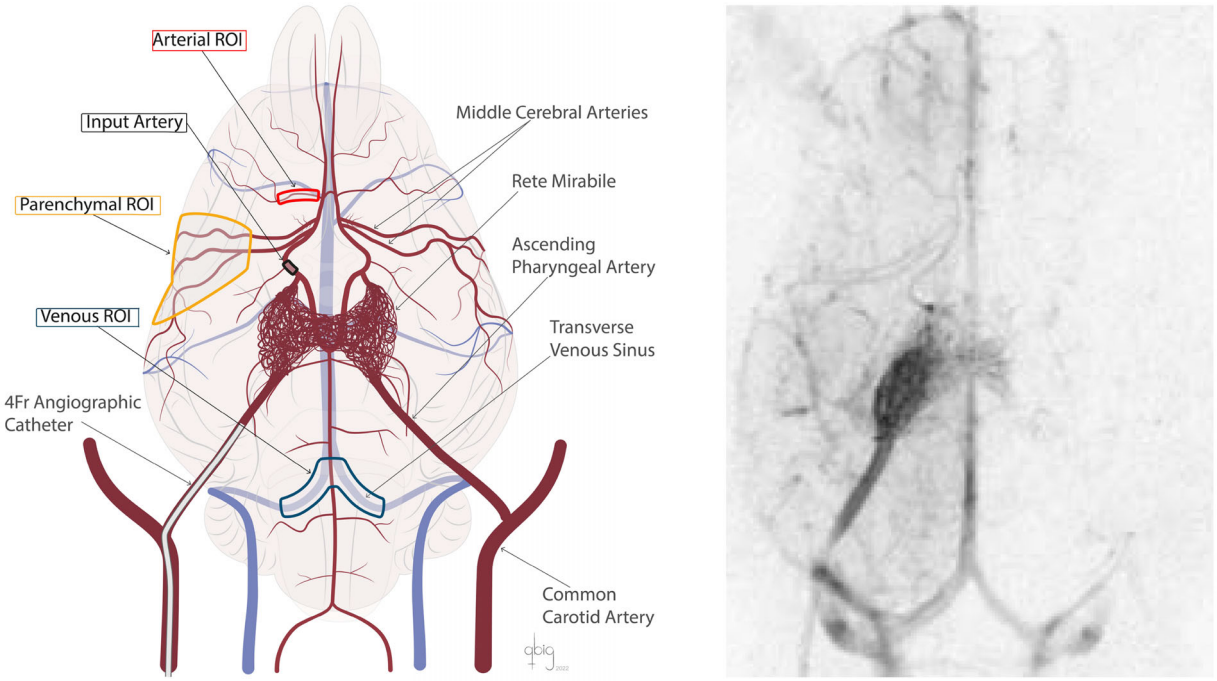

(a) Swine cerebral vasculature model.

(b) MinIP of a swine DSA.

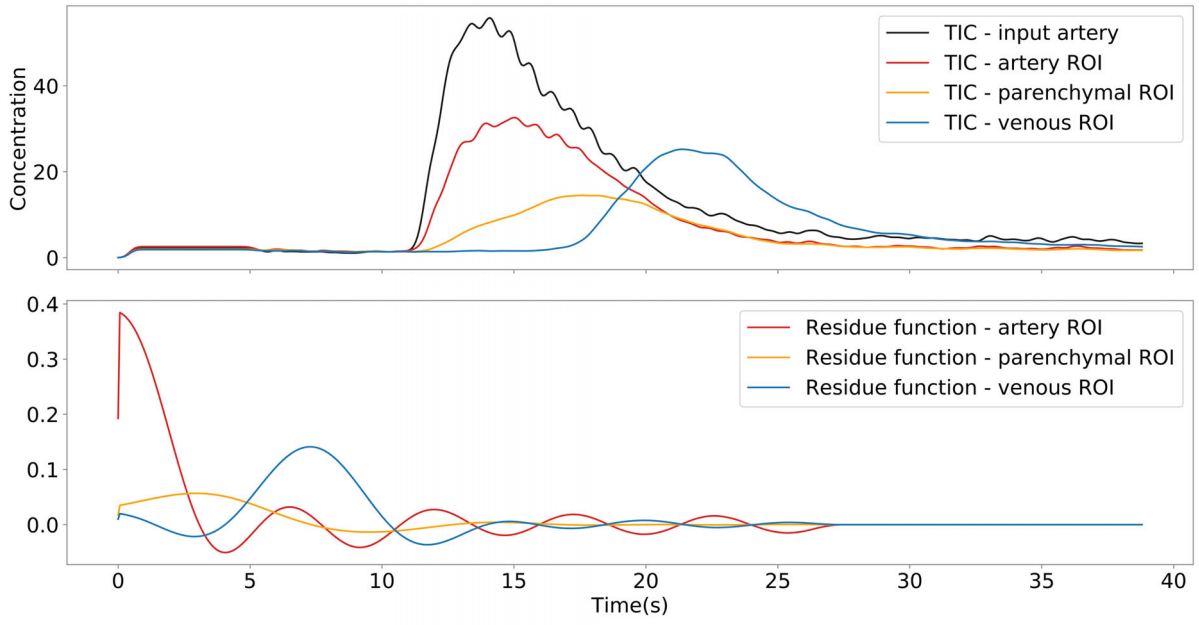

(c) Example TICs and residue functions of the selected ROIs.

FIGURE 2 Swine cerebral vasculature model, MinIP, example TICs, and residue functions.

the ascending pharyngeal artery, which connects the common carotid artery and the rete mirabile, was cannulated with a 4F angiographic catheter (4F STR Impress, 411038STS, Merit Medical, Utah, USA). The catheter was advanced under fluoroscopy using a standard over-the-wire technique through a 6F sheath (Super Arrow-Flex, CL-07624, Teleflex, Pennsylvania, USA) in the right femoral artery. Non-diluted radiopaque contrast (Visipaque 320 mg Iodixanol/ml, GE Healthcare, The Netherlands) was injected with an automated contrast injector (Mark V ProVis, Medrad, Pennsylvania, USA) to acquire 2D ventro-dorsal DSA images (Artis Zee,

TABLE 2 Summary of injection protocols in this study

Group	Volume (mL)	Flow rate (mL/s)	Duration (seconds)	Injection delay (seconds)	Acquisitions
1	Constant 2.4	Constant 0.6	Constant 4	Constant 5	6
2	Constant 2.4	Variable [0.3, 0.4, 0.6]	Variable [4, 6, 8]	Random [0-10]	3
	Variable [1.6, 2, 2.4]	Constant 0.4	Variable [4, 5, 6]	Random [0-10]	3
3	Variable [1.8, 2.4, 3.0, 3.6]	Constant 0.6	Variable [3, 4, 5, 6]	Random [0-10]	4
	Variable [2.4, 3.2, 4]	Constant 0.8	Variable [3, 4, 5]	Random [0-10]	3
4	Variable [1.6, 2, 2.4, 2.8, 3.2]	Variable [0.4, 0.5, 0.6, 0.7, 0.8]	Constant 4	Random [0-10]	5
	Variable [1.5, 1.8, 2.1, 2.4]	Variable [0.5, 0.6, 0.7, 0.8]	Constant 3	Random [0-10]	4

Note: These experiments were performed on both swine hemispheres, and a few experiments with identical injection protocols were shared between groups, resulting in a total of 46 acquisitions.

Siemens Healthineers, The Netherlands). To avoid contrast superimposition from the contralateral hemisphere, antero-posterior (AP) DSA series were acquired. The acquired series are all 15 frames per second (fps) and of 1024×1024 pixels per frame.

To investigate the reliability of perfusion DSA, multiple series of AP view DSA acquisitions were obtained with various injection protocols. In this experiment, we consider the following control variables: injection volume, flow rate, duration of injection, and injection delay. Table 2 summarizes the list of designed injection protocols. Between acquisitions, a 5-min gap was reserved to minimize the residual contrast in the brain. To guarantee the completeness of the venous phase, we kept each DSA acquisition long enough with an average duration of 35 s (15 fps). Note that all the acquisitions in Table 2 were performed on both hemispheres independently to increase the experiment sample size, which resulted in 46 DSA acquisitions.

To verify the sensitivity of perfusion DSA to detect alterations in cerebral hemodynamics, we used a second animal (model #2) with focal cerebral ischemia followed by recanalization. The animal underwent a craniotomy to occlude the right-sided middle cerebral arteries (MCA) with aneurysm clips. Clips were released after 1-h occlusion to allow recanalization for 4 h. The DSA images were obtained at baseline, during occlusion, and at 2 and 4 h after recanalization with an automated injection of 3 mL of contrast at 0.6 mL/s (5-s duration).

3 | EXPERIMENTS AND RESULTS

3.1 | Dependence of perfusion parameters on injection protocols

First, we investigate the impact of variation in contrast injection protocols on perfusion parameters derived directly from the TIC (i.e., AUC, peak concentration, TTP) and deconvolution-based parameters (i.e., CBV_{DSA}, CBF_{DSA}, Tmax, MTT_{DSA}). In order to quantitatively assess the variance of perfusion parameters, we select three representative regions of interest (ROIs) in the arterial, parenchymal, and venous areas of the computed parametric images. The selected ROIs are shown in Figure 2a, which are consistent across all DSA acquisitions. The masks were carefully optimized per DSA series to compensate for any small swine movements between acquisitions.

3.1.1 | Regional quantitative analysis

Detailed quantitative comparisons of TIC-derived and deconvolution-based parameters extracted from those ROIs are summarized in Table 3 (left hemisphere and right hemisphere). When comparing parameters derived from similar injection protocols to those derived from varying protocols, the increase in normalized standard deviation (SD) among deconvolution-based parameters is smaller than directly TIC-derived parameters by a factor of 2 or more (i.e., AUC vs. CBV_{DSA}, peak intensity vs. CBF_{DSA}). This holds for the results of both hemispheres. While CBV_{DSA} and CBF_{DSA} are relative values to the AIF, Tmax and MTT_{DSA} are absolute in seconds. It may be noticed that the SD difference of Tmax and MTT_{DSA} are large; they are mainly attributed to the accidentally small SD of constant protocols. When examining the SD in the variable group, the SD of Tmax for example approximately matches the SD of TTP in the constant group, indicating that the Tmax is hardly affected by injection delay. Another observation is that the mean values between constant and variable groups are closer for deconvolution-based parameters than for TIC-derived parameters. This also demonstrates that the deconvolution-based parameters are less dependent on injection protocols.

3.1.2 | Effect of series time resolution

To further understand the boundaries of such improved quantitative properties, we linearly downsampled the time axis of the acquired series to obtain various frame rates (i.e., [0.25, 0.5, 1–15] fps) and compared

TABLE 3 Overview of TIC-derived and deconvolution-based parameters extracted from three ROIs (artery, parenchymal, and vein) of both hemispheres of the swine in conjunction with constant and variable injection protocols. Diff (SD) denotes the relative increase in SD from the constant to the variable group. For AUC, CBV_{DSA}, and CBF_{DSA}, the ratio of SD to mean is reported in parenthesis. TTP, Tmax, and MTT_{DSA} are expressed in seconds

(a) Left hemisphere

ROI	Injection protocol	TIC-derived parameters			Deconvolution-based parameters			
		$AUC_{(10^2)}$	Peak	$TTP_{(s)}$	$CBV_{DSA(10^{-2})}$	$CBF_{DSA(10^{-2})}$	$Tmax_{(s)}$	$MTT_{DSA(s)}$
Artery	Constant	$55.3\pm7.0_{(13\%)}$	$34.1\pm2.7_{(8\%)}$	17.6±0.6	$28.4\pm4.0_{(14\%)}$	$13.5\pm1.3_{(10\%)}$	0.1±0.0	2.1±0.1
	Variable	$66.4\pm27.1_{(41\%)}$	$43.0\pm13.3_{(31\%)}$	18.0±3.5	$29.8\pm5.7_{(19\%)}$	$13.9\pm1.9_{(13\%)}$	0.1±0.0	2.2±0.4
	Diff (SD)	3.9	5.0	6.0	1.4	1.4	2.4	4.9
Parenchymal	Constant	$35.4\pm1.0_{(3\%)}$	$22.7\pm0.7_{(3\%)}$	21.0±0.5	$19.0\pm0.7_{(4\%)}$	$4.7\pm0.1_{(2\%)}$	2.5±0.2	3.7±0.1
	Variable	$40.4\pm13.7_{(34\%)}$	$25.8\pm6.9_{(27\%)}$	20.9±3.3	$19.3\pm2.8_{(15\%)}$	$4.8\pm0.4_{(9\%)}$	2.1±0.4	3.8±0.7
	Diff (SD)	13.7	10.3	6.2	3.8	4.7	2.5	6.7
Vein	Constant	$42.8\pm3.2_{(7\%)}$	$34.0\pm2.6_{(8\%)}$	25.7±0.6	$24.3\pm2.3_{(10\%)}$	$6.0\pm0.4_{(7\%)}$	8.8±0.3	3.7±0.2
	Variable	$46.2\pm17.2_{(37\%)}$	$36.9\pm12.7_{(34\%)}$	24.9±3.3	$24.0\pm4.5_{(19\%)}$	$5.5\pm0.9_{(16\%)}$	7.7±0.5	4.1±1.2
	Diff (SD)	5.5	5.0	5.7	1.9	2.1	2.1	5.8

(b) Right hemisphere

ROI	Injection protocol	TIC-derived parameters			Deconvolution-based parameters			
		$AUC_{(10^2)}$	Peak	$TTP_{(s)}$	$CBV_{DSA(10^{-2})}$	$CBF_{DSA(10^{-2})}$	$Tmax_{(s)}$	$MTT_{DSA(s)}$
Artery	Constant	$40.1\pm1.9_{(5\%)}$	$30.1\pm1.2_{(4\%)}$	16.6±0.6	$35.6\pm2.0_{(6\%)}$	$16.1\pm0.5_{(3\%)}$	0.2±0.1	2.2±0.2
	Variable	$49.2\pm17.2_{(35\%)}$	$33.1\pm9.2_{(28\%)}$	18.5±3.1	$35.7\pm3.8_{(11\%)}$	$15.4\pm1.8_{(11\%)}$	0.2±0.1	2.3±0.3
	Diff (SD)	9.0	7.7	5.7	1.9	3.2	1.7	1.3
Parenchymal	Constant	$22.9\pm2.1_{(9\%)}$	$15.8\pm2.2_{(14\%)}$	17.8±0.5	$20.4\pm1.2_{(6\%)}$	$5.7\pm0.5_{(9\%)}$	1.4±0.4	3.2±0.0
	Variable	$29.3\pm10.4_{(36\%)}$	$19.8\pm6.8_{(34\%)}$	20.2±3.6	$21.3\pm2.2_{(10\%)}$	$5.7\pm1.0_{(17\%)}$	1.6±0.6	3.4±0.4
	Diff (SD)	5.0	3.1	7.4	1.8	1.9	1.6	20.2
Vein	Constant	$33.6\pm1.5_{(4\%)}$	$26.7\pm2.1_{(8\%)}$	22.1±0.5	$31.7\pm1.2_{(4\%)}$	$8.8\pm0.8_{(9\%)}$	7.2±0.1	3.4±0.3
	Variable	$42.6\pm16.0_{(37\%)}$	$31.3\pm10.5_{(33\%)}$	24.6±3.5	$32.7\pm3.5_{(11\%)}$	$7.5\pm1.8_{(24\%)}$	7.1±0.6	4.2±1.2
	Diff (SD)	10.8	4.9	7.2	2.9	2.4	11.7	3.8

Abbreviations: AUC, area under the curve; CBV, cerebral blood volume; CBV, cerebral blood volume; DSA, digital subtraction angiography; ROI, region of interest; SD, standard derivation; TIC, time intensity curve; TTP, time-to-peak.

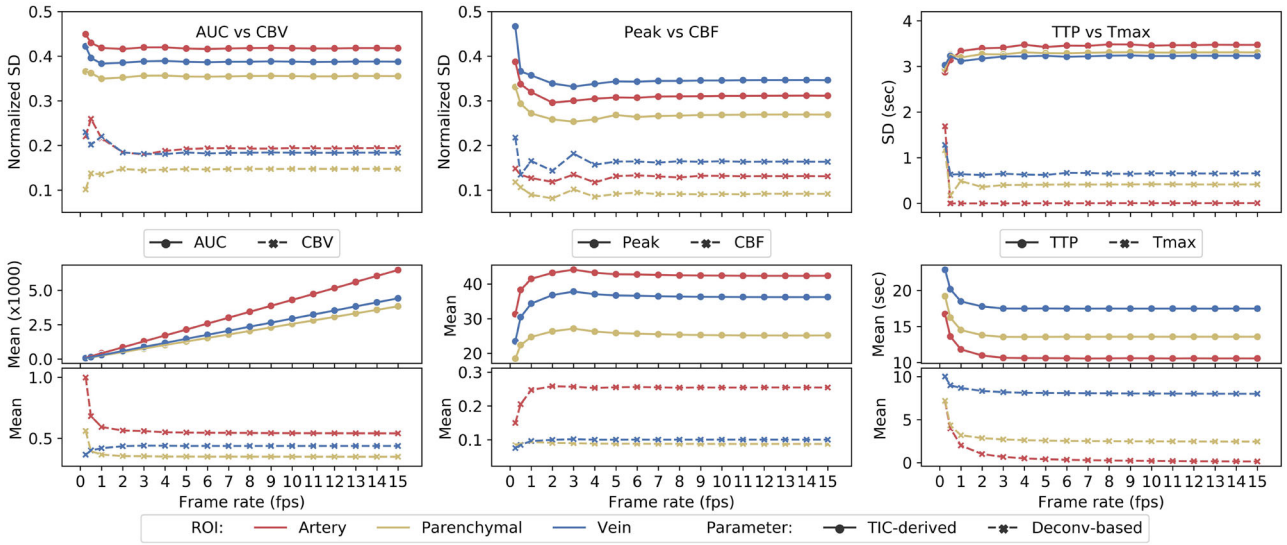

FIGURE 3 Comparison of parameter variabilities across frame rates.

the variability of TIC-derived and deconvolution-based parameters. The variability is measured by the SD of TTP and Tmax in seconds, and by normalized SD of AUC, Peak intensity, CBV_{DSA}, and CBF_{DSA}. Figure 3 shows in the first row the differences of (normalized) SD across frame rates in all parameters within three ROIs of the left hemisphere. In the second row, it visualizes the corresponding mean values of all parameters. Specifically, we observe consistently reduced SD in deconvolution-based parameters versus TIC-derived parameters, with higher fluctuations at < 1 fps. Under those low time resolutions, the accuracy and robustness of both TTP and Tmax (in seconds) could collapse because of the large time gap between frames (e.g., with 0.25 fps, 1 frame represents 4s). Comparing the mean parameter values, both types of parameters remain mostly stable until the frame rate drops below 1 fps. This is likely caused by the increased instability in the AIF and TICs due to insufficient sampling rate relative to contrast flow and too few frames.

3.2 | Sensitivity of perfusion parameters

Next, we investigate whether deconvolution-based parameters remain sensitive to alterations of brain conditions. To answer this question, we analyzed the perfusion parameters of swine #2. Figure 4 visually compares the parametric images of swine #2 under various brain conditions, that is, baseline, 1 h after induced MCA occlusion, 2 h after reperfusion, and 4 h after reperfusion. Quantitatively speaking, CBV_{DSA} and CBF_{DSA} values fall by a factor of 2 and 4 respectively in the parenchymal region after occlusion, these changes are larger than those of the AUC and peak intensity respectively. With regard to Tmax and MTT_{DSA}, the occluded parenchymal region received insufficient signal (NoSig) due to too few non-zero values. Interestingly, higher CBF_{DSA} was observed in the arterial and parenchymal ROIs at reperfused 2 h and 4 h sequences compared to baseline sequence (Table 4), potentially reflecting hyperperfusion. This is clear from the increased CBF_{DSA} and CBV_{DSA}, but not obvious from TIC-derived parameters.

4 | DISCUSSION

With two swine models, we have assessed the independence of deconvolution-based perfusion angiography with respect to variations in injection parameters, as well as the sensitivity to cerebral hemodynamic changes. This adds to the fundamental understanding of the properties of perfusion angiography. Quantitative perfusion angiography would allow automated intra-patient comparisons of perfusion characteristics before, during, and after endovascular interventions, providing insights for prompt quantitative feedback on treatment effects and functional outcome prediction. This may further promote relevant clinical applications in computer-aided diagnosis and image-guided interventions.

Deconvolution-based perfusion angiography holds greatly improved consistency with respect to injection protocols. Nevertheless, it is not fully quantitative and independent of the injection profile. As shown in Table 3, the SD of CBV_{DSA}, CBF_{DSA}, Tmax, and MTT_{DSA} are consistently higher in the variable group than in the constant group. This might be attributed to multiple factors. First, the 2D projective nature of DSA causes overlap of cerebral vessels and tissue. This not only prevents

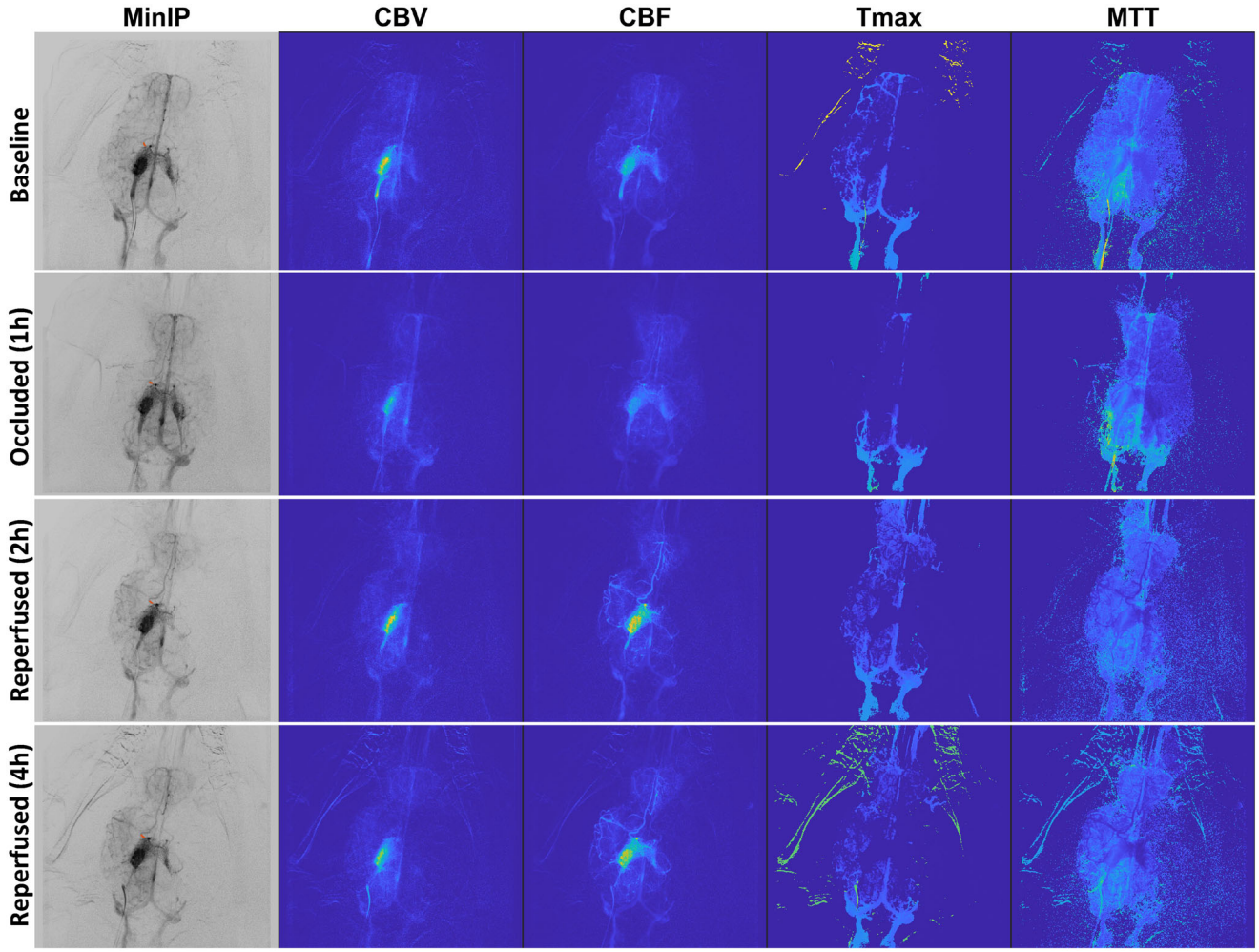

FIGURE 4 Perfusion angiography images of swine model #2 under various brain conditions.

TABLE 4 Overview of perfusion parameters extracted from three ROIs (artery, parenchymal, and vein) of swine #2 under four different brain conditions. NoSig: insufficient signal

ROI	Brain condition	TIC-derived parameters			Deconvolution-based parameters			
		$AUC_{(10^2)}$	Peak	$TTP_{(s)}$	$CBV_{DSA(10^{-2})}$	$CBF_{DSA(10^{-2})}$	$Tmax_{(s)}$	$MTT_{DSA\ (s)}$
Artery	Baseline	53.62	33.43	11.24	33.25	11.07	0.15	2.98
	Occluded(1h)	66.69	41.60	11.57	20.97	11.88	0.13	1.79
	Reperfused(2h)	40.97	30.43	9.40	27.59	15.06	0.21	1.93
	Reperfused(4h)	42.57	32.03	9.03	24.22	15.46	0.14	1.63
Parenchymal	Baseline	37.44	22.22	13.57	21.55	5.45	0.65	3.46
	Occluded(1h)	23.44	10.49	18.60	**12.02**	**1.43**	**NoSig**	**NoSig**
	Reperfused(2h)	32.39	23.76	10.05	23.39	8.94	1.00	2.76
	Reperfused(4h)	36.58	26.67	10.30	23.32	9.42	0.72	2.65
Vein	Baseline	59.32	35.58	16.45	29.69	5.69	6.82	4.97
	Occluded(1h)	74.37	49.39	15.86	42.89	5.32	5.05	7.95
	Reperfused(2h)	40.14	31.32	13.16	30.86	7.66	5.45	3.92
	Reperfused(4h)	43.93	33.29	13.20	32.57	7.46	5.23	4.19

Abbreviations: AUC, area under the curve; CBV, cerebral blood volume; CBV, cerebral blood volume; DSA, digital subtraction angiography; ROI, region of interest; SD, standard derivation; TIC, time intensity curve; TTP, time-to-peak.

the exact calculation of contrast volume, but also introduces noise in deconvolution. Besides, the correlation between the ratio of perfusion change from the input artery and a region of interest might not be fully linear. Third, the deconvolution-based method is noise sensitive.[2,41] Lastly, our model of X-ray is idealized, and in practice post-processing techniques may be applied by the vendors to optimize visual appearance which may affect quantification. In the future, to further validate the quantitative property of perfusion angiography in clinical practice, a promising research direction would be to visualize and quantitatively analyze differences between perfusion DSAs of the same subject acquired at different time points or brain conditions, perhaps even from different vendors.

For robustness, a temporal Gaussian filter was applied before SVD-based deconvolution as a means of regularization. No sophisticated postprocessing steps were taken other than suppressing and masking out near-zero CBF_{DSA} values. Alternative processing techniques are available, which may further improve the quality of perfusion images, such as nondeconvolution-based methods,[42–44] gamma fitting for TIC denoising, and expectation-maximization (EM)[45] for TIC mixture separation. These approaches were not pursued as a primary concern in this study.

Perfusion imaging and perfusion parameters typically refer to physiological blood flow quantities estimated by 3D CT/MRI, rather than by DSA due to its projective nature. In this sense, deconvolution-based parameters in DSA arguably correlate, but may not accurately describe the underlying physiological perfusion property without any bias. Although this study has shown improved quantitative properties of deconvolution-based parameters, we did not further validate the association between such parameters with their corresponding physiological flow characteristics because of a lack of ground truth perfusion data. To emphasize this conceptual difference, we therefore used CBV_{DSA}, CBF_{DSA}, and MTT_{DSA} to avoid possible misinterpretation.

This study holds some limitations. Firstly, the quantitative analyses were performed on only two swine with a limited number of DSA acquisitions. As a result, statistical tests were not feasible. Besides, due to the limited accuracy of the automated contrast injector, there is a slight discrepancy without an obvious pattern between the setting (Table 2) and the actual injection parameters during DSA image acquisition which may affect the of perfusion parameters. Thirdly, even though vital signs were continuously monitored, the physiological conditions are complex and multifactorial, and thus may not necessarily remain stable throughout the experiments.

As an animal study, a few differences need to be noted when interpreting the results in clinical practice: (1) the cerebral vasculature of swine differs from humans in terms of the presence of the rete mirabile; (2) the acquired swine DSA series hold high time resolution (i.e., 15 fps), while the frame rate of perioperatively acquired DSA could be as low as 1–4 fps and often varies within one acquisition. This restriction in time resolution may impact the quality of perfusion parameters to some extent; (3) The experiments focused on the AP view of swine angiograms; this was to avoid the observed contrast superimposition from the contralateral hemisphere. Extrapolation of the findings from animal to human cases requires further validation. And therefore, as future work, extended experiments on large scales of real patient images would consolidate and further generalize the presented findings.

5 | CONCLUSION

We presented an animal study that demonstrates the superior independence and sensitivity of deconvolution-based perfusion angiography (CBV_{DSA}, CBF_{DSA}, Tmax, MTT_{DSA}) over TIC-derived parameters (AUC, peak intensity, TTP) in DSA, considering the general inconsistency of injection protocols between acquisitions. These findings may further facilitate quantitative assessments of perfusion angiography in endovascular interventions.

ACKNOWLEDGMENTS

The current work on perforation detection was supported by Health-Holland (TKI Life Sciences and Health) through the Q-Maestro project under Grant EMCLSH19006 and Philips Healthcare (Best, The Netherlands).

We also acknowledge the financial support of the Netherlands Cardiovascular Research Initiative which is supported by the Dutch Heart Foundation (CVON2015-01: CONTRAST), the support of the Brain Foundation Netherlands (HA2015.01.06), and the support of Health-Holland, Top Sector Life Sciences & Health (LSHM17016), Medtronic, Cerenovus and Stryker European Operations BV. The collaboration project is additionally financed by the Ministry of Economic Affairs by means of the PPP Allowance made available by the Top Sector Life Sciences & Health to stimulate public-private partnerships.

We thank Jadey Raben and Romy van Noort for their assistance with the animal experiments.

CONFLICT OF INTEREST STATEMENT

Wiro Niessen is founder, scientific lead, and shareholder of Quantib BV. Danny Ruijters is an employee of Philips Healthcare.

REFERENCES

1. Hoeffner EG, Case I, Jain R, et al. Cerebral perfusion ct: technique and clinical applications. *Radiology*. 2004;231:632-644.

2. Konstas A, Goldmakher G, Lee TY, Lev M. Theoretic basis and technical implementations of ct perfusion in acute ischemic stroke, part 1: theoretic basis. *Am J Neuroradiol*. 2009;30:662-668.
3. Caroff J, Jittapiromsak P, Ruijters D, et al. Use of time attenuation curves to determine steady-state characteristics before c-arm ct measurement of cerebral blood volume. *Neuroradiology*. 2014;56:245-249.
4. Donahue J, Wintermark M. Perfusion ct and acute stroke imaging: foundations, applications, and literature review. *J Neuroradiol*. 2015;42:21-29.
5. Calamante F, Thomas DL, Pell GS, Wiersma J, Turner R. Measuring cerebral blood flow using magnetic resonance imaging techniques. *J Cereb Blood Flow Metab*. 1999;19:701-735.
6. Barbier EL, Lamalle L, Décorps M. Methodology of brain perfusion imaging. *J Magn Reson Imaging*. 2001;13:496-520.
7. Østergaard L. Cerebral perfusion imaging by bolus tracking. *Top Magn Reson Imaging*. 2004;15:3-9.
8. Higashida RT, Furlan AJ. Trial design and reporting standards for intra-arterial cerebral thrombolysis for acute ischemic stroke. *Stroke*. 2003;34:e109-e137.
9. Investigators IIT,. The interventional management of stroke (ims) II study. *Stroke*. 2007;38:2127-2135.
10. Almekhlafi MA, Mishra S, Desai JA, et al. Not all "successful" angiographic reperfusion patients are an equal validation of a modified TICI scoring system. *Interv Neuroradiol*. 2014;20:21-27.
11. Liebeskind DS, Bracard S, Guillemin F, et al. eTICI reperfusion: defining success in endovascular stroke therapy. *J Neurointerv Surg*. 2019;11:433-438.
12. Su R, Cornelissen SA, Van Der Sluijs M, et al. autoTICI: Automatic brain tissue reperfusion scoring on 2D DSA images of acute ischemic stroke patients. *IEEE Trans Med Imaging*. 2021;40:2380-2391.
13. Rahmany I, Guetari R, Khlifa N. A fully automatic based deep learning approach for aneurysm detection in DSA images. *2018 IEEE international conference on image processing, applications and systems (IPAS)*. IEEE; 2018:303-307.
14. Nielsen M, Waldmann M, Sentker T, Frölich A, Fiehler J, Werner R. Time matters: handling spatio-temporal perfusion information for automated TICI scoring. In: *International Conference on Medical Image Computing and Computer-Assisted Intervention*. Springer; 2020:86-96.
15. Su R, van der Sluijs M, Cornelissen SA, et al. Spatio-temporal deep learning for automatic detection of intracranial vessel perforation in digital subtraction angiography during endovascular thrombectomy. *Med Image Anal*. 2022;77:102 377.
16. Unberath M, Hajek J, Geimer T, Schebesch F, Amrehn M, Maier A. Deep learning-bases inpainting for virtual DSA. *IEEE Nuclear Science Symposium and Medical Imaging Conference*. 2017:1-2.
17. Gao Y, Song Y, Yin X, et al. Deep learning-based digital subtraction angiography image generation. *Int J Comput Assist Radiol Surg*. 2019;14:1775-1784.
18. Kimura R, Teramoto A, Ohno T, Saito K, Fujita H. Virtual digital subtraction angiography using multizone patch-based U-net. *Phys Eng Sci Med*. 2020;43:1305-1315.
19. Ueda D, Katayama Y, Yamamoto A, et al. Deep learning–based angiogram generation model for cerebral angiography without misregistration artifacts. *Radiology*. 2021;299:675-681.
20. Mittmann BJ, Braun M, Runck F, et al.Deep learning-based classification of dsa image sequences of patients with acute ischemic stroke. *Int J Comput Assist Radiol Surg*. 2022:1-9.
21. Zhang M, Zhang C, Wu X, et al. A neural network approach to segment brain blood vessels in digital subtraction angiography. *Comput Methods Programs Biomed*. 2020;185:105 159.
22. Meng C, Sun K, Guan S, Wang Q, Zong R, Liu L. Multiscale dense convolutional neural network for dsa cerebrovascular segmentation. *Neurocomputing*. 2020;373:123-134.
23. Su R, van der Sluijs M, Cornelissen S, et al. Spatio-temporal u-net for cerebral artery and vein segmentation in digital subtraction angiography. *arXiv preprint arXiv:2208.02355*. 2022.
24. van Asperen V, van den Berg J, Lycklama F, et al. Automatic artery/vein classification in 2D-DSA images of stroke patients. In: *Medical Imaging 2022: Image-Guided Procedures, Robotic Interventions, and Modeling*. Vol 12034. SPIE; 2022:366-377.
25. Bogunovic H, Loncaric S. Estimating perfusion using x-ray angiography. In: *ISPA 2005. Proceedings of the 4th International Symposium on Image and Signal Processing and Analysis, 2005*. IEEE; 2005:147-150.
26. König M. Brain perfusion CT in acute stroke: current status. *Eur J Radiol*. 2003;45:S11-S22.
27. Strother C, Bender F, Deuerling-Zheng Y, et al. Parametric color coding of digital subtraction angiography. *Am J Neuroradiol*. 2010;31:919-924.
28. Scalzo F, Liebeskind DS. Perfusion angiography in acute ischemic stroke. *Comput Math Methods Med*. 2016;2016:2478324.
29. Levitt MR, Morton RP, Haynor DR, et al. Angiographic perfusion imaging: Real-time assessment of endovascular treatment for cerebral vasospasm. *J Neuroimaging*. 2014;24:387-392.
30. Thurner A, Augustin AM, Bley TA, Kickuth R. 2D-perfusion angiography for intra-procedural endovascular treatment response assessment in chronic mesenteric ischemia: a feasibility study. *BMC Med Imaging*. 2022;22:1-12.
31. Rava RA, Mokin M, Snyder KV, et al. Performance of angiographic parametric imaging in locating infarct core in large vessel occlusion acute ischemic stroke patients. *J Med Imaging*. 2020;7:016 001.
32. Rava RA, Allman AB, Rudin S, Ionita CN. Effect of truncated singular value decomposition on digital subtraction angiography derived angiographic parametric imaging maps. *Medical Imaging 2020: Physics of Medical Imaging*. Vol 11312. SPIE; 2020:756-766.
33. Ahmed A, Deuerling-Zheng Y, Strother C, et al. Impact of intra-arterial injection parameters on arterial, capillary, and venous time-concentration curves in a canine model. *Am J Neuroradiol*. 2009;30:1337-1341.
34. Takagi S, Hanasaki N. Relationship between injection rate and contrast enhancement on three-dimensional digital subtraction angiography of the cerebral arteries. *J Belg Soc Radiol*. 2018;102(1):76.
35. Meier P, Zierler KL. On the theory of the indicator-dilution method for measurement of blood flow and volume. *J Appl Physiol*. 1954;6:731-744.
36. Brix G, Griebel J, Kiessling F, Wenz F. Tracer kinetic modelling of tumour angiogenesis based on dynamic contrast-enhanced ct and mri measurements. *Eur J Nucl Med Mol Imaging*. 2010;37:30-51.
37. Fieselmann A, Kowarschik M, Ganguly A, Hornegger J, Fahrig R. Deconvolution-based ct and mr brain perfusion measurement: theoretical model revisited and practical implementation details. *Int J Biomed Imaging*. 2011;2011:467563.
38. Stewart G. Researches on the circulation time in organs and on the influences which affect it: Parts I.–III. *J Physiol*. 1893;15:1.
39. Frangi AF, Niessen WJ, Vincken KL, Viergever MA. Multiscale vessel enhancement filtering. In: *International Conference on Medical Image Computing and Computer-Assisted Intervention*. Springer; 1998:130-137.
40. Taha A, Bobi J, Dammers R, et al. Comparison of large animal models for acute ischemic stroke: Which model to use? *Stroke*. 2022;53:1411-1422.
41. Østergaard L, Weisskoff RM, Chesler DA, Gyldensted C, Rosen BR. High resolution measurement of cerebral blood flow using intravascular tracer bolus passages. part I: mathematical approach and statistical analysis. *Magn Reson Med*. 1996;36:715-725.

42. Hsieh J. *Computed Tomography: Principles, Design, Artifacts, and Recent Advances*. SPIE; 2003.
43. Axel L. Cerebral blood flow determination by rapid-sequence computed tomography: theoretical analysis. *Radiology*. 1980;137:679-686.
44. Klotz E, König M. Perfusion measurements of the brain: using dynamic ct for the quantitative assessment of cerebral ischemia in acute stroke. *Eur J Radiol*. 1999;30:170-184.
45. Sundberg R. Maximum likelihood theory for incomplete data from an exponential family. *Scand J Stat*. 1974:49-58.

How to cite this article: Su R, van der Sluijs PM, Bobi J, et al. Towards quantitative digital subtraction perfusion angiography: An animal study. *Med Phys*. 2023;1-12.
https://doi.org/10.1002/mp.16473